Journal of Computational Physics **174,** 208–225 (2001)
doi:10.1006/jcph.2001.6902, available online at http://www.idealibrary.com on IDEAL®

# On the Use of a Heterogeneous MIMD–SIMD Platform to Simulate the Dynamics of Globular Clusters with a Central Massive Object

R. Capuzzo Dolcetta,* N. Pucello,†,‡ V. Rosato,†,§ and F. Saraceni†

*Physics Department, Universitá di Roma "La Sapienza," P.le A. Moro 2, 00185 Rome, Italy;
†ENEA, Casaccia Research Center, HPCN Project, P.O. Box 2400, 00100 Rome, Italy;
‡CASPUR, Universitá di Roma "La Sapienza," P.le A. Moro 2, 00185 Rome, Italy;
and, §Istituto Nazionale di Fisica della Materia (INFM), UdR Rome, Italy

Received October 12, 2000; revised August 6, 2001

The dynamics of a large stellar (globular) cluster containing $N = 128{,}000$ stars has been simulated using a direct summation ($O(N^2)$) method and a heterogeneous platform. Preliminary simulations have been carried out on model systems with and without the presence, in their center of mass, of a black hole whose mass has been varied from 0.02 to 0.1 times the total mass of the cluster. These simulations followed the evolution of the globular cluster in order to describe its dynamics over an interval of time sufficiently large with respect to the internal crossing time. Computations have demonstrated that the platform heterogeneity, allowing a very efficient use of the computational resources, can be considered a key feature for sustaining large computational loads. Our results show that the massive object in the center of the cluster alters the surrounding star distribution very quickly; the following evolution is much slower, as it occurs via two-body collisional relaxation. 

*Key Words:* self-gravitating $N$-body simulations; heterogeneous MIMD–SIMD platform.

## 1. INTRODUCTION

Although the main trend of high-performance computing seems to focus on the assembly of larger and larger massively parallel platforms (e.g., the US ASCI platforms [1]), the design, the realization, and the deployment of *special-purpose* (nonprogrammable, i.e., *dedicated*) or *specialized* hardware is at the center of a renewed interest, particularly in the field of scientific applications.

In recent years, several scientific domains have received a substantial boost by using specialized (or dedicated) hardware: the lattice quantum chromodynamics model, thanks to the platforms realized in the frame of the APE [2, 3] and the Columbia projects [4],



0021-9991/01 $35.00

has significantly increased its prediction power. Computational astrophysics has received significant benefits from the use of the dedicated (or special-purpose) platform GRAPE (GRAvity piPE) [5, 6], which is able to sustain a computational power of the order of teraflops/second in gravitational $O(N^2)$ calculations, being a board explicitly built to evaluate efficiently the distances between pairs. More recently, the use of more complex $N$-body codes requiring a substantial number of $O(N \log N)$ calculations has triggered the development of new dedicated hardware, built by exploiting new programmable devices (FPGA), used in combination with the GRAPE machine (AHA–GRAPE project [7]).

Other dedicated and specialized hardware devices have been also conceived to improve the sustained computational power of numerical modeling in the field of three-dimensional (3D) Ising models [7, 8], in that of molecular orbital calculation in quantum chemistry [10], and in molecular dynamics simulation of complex systems (e.g., biological matter) [11]. This list, far from being exhaustive, puts together both dedicated (nonprogrammable) and specialized (programmable) devices. Whereas dedicated architectures cannot be deployed in application fields different from those for which they were conceived, specialized hardware (like, e.g., the APE platform) can be usefully deployed in different application fields. For example, the hybrid platform PQE1 (described in Section 2 and used for the computations in this paper) has been used on a variety of scientific problems, including chemistry [12], electromagnetism [23], environmental modeling [14], and material sciences [15], showing good performance and flexibility. In this paper we apply it for the first time to another, quite different, field: that of stellar dynamics, attacking the classic gravitational $N$-body problem without approximations in the particle–particle force evaluation. In order to take the most from the dedicated/specialized platforms, their power is often exploited in conjunction with a host platform (a simple workstation or a general-purpose parallel platform). In this configuration, the specialized/dedicated platform can be regarded as a smart coprocessor of the host to which specific parts of the computation can be allotted. The resulting hardware is, thus, the *heterogeneous* sum of general-purpose and specialized/dedicated machines; it allows very efficient calculations, as different (in terms of algorithmic structure) parts of the code can be allotted to the parts of the architecture most suited to mapping their specific computational complexity.

This work has addressed two different issues. The first is concerned with the astrophysical problem of simulating, with a reliable model, the dynamics of a large stellar cluster whose central region hosts a massive object (like a black hole). The aim is to apply these numerical models, which are approximated just in regard to the numerical time integration scheme and in a smoothing of the interaction potential, to a time of the order of 20 crossing times (the *crossing time* $t_c = 2R/\langle v \rangle$ is the time required by the typical object of the system to cross the system, i.e., to cover a length scale equal to twice the initial radius of the system $R$, with a velocity $\langle v \rangle$ equal to the average star's velocity). Actually, we estimate this interval of time as sufficient to sum up collective effects even if it is still short with respect to the two-body relaxation time that is the "fine grain"-dependent time scale.

The representation of a large self-gravitating system with a particle model is, indeed, limited by the number, $N$, of particles that can be numerically handled; astrophysical self-gravitating systems span a range of $N$ from 2 to $10^{12}$ (see Table I). The direct evaluation (i.e., that obtained by the sum of the contributions to the force on an object of the system made by all the others without approximations, with the exception of a possible smoothing of the interaction potential) of the $N$-body mutual forces implies a restrictive limit to the number of bodies which can be treated (being the algorithm of an $O(N^2)$ scaling). At present,

**TABLE I**

**The Range of the Number of Stars in Several Astrophysical Systems, the Numerical Approximation Commonly Used by Simulations, and the Two-Body Relaxation Time of the Object in Units of Crossing Time**

| Stellar system | $N$ | Numerical approximation | $t_{rel}/t_c$ |
|---|---|---|---|
| OB associations | 10–100 | Direct | 1–5 |
| Open clusters | 100–1000 | Direct | 5–30 |
| Globular clusters | $10^5$–$10^6$ | Direct | $10^3$–$10^4$ |
| Dwarf galaxies | $10^8$ | Tree algorithm, PM, $P^3M$ | $10^7$ |
| Galaxies | $10^{10}$–$10^{12}$ | Tree algorithm, PM, $P^3M$ | $10^8$–$10^9$ |

*Note.* The value of the relaxation time $t_{rel}$ has been expressed in terms of the crossing time $t_c$ by means of the relation $t_{rel} = 0.1\frac{N}{\ln N}t_c$ (see [16]).

the largest value of $N$ that can be approached with such methods, on large computational platforms, is $N \simeq 10^5$. This means that a one-to-one representation of stars with simulating particles is now possible only for stellar systems up to a typical (not too populous) globular cluster (see Table I). Larger systems can be treated with approximate methods, such as *tree codes* [17] and *particle–mesh* (PM) and *particle–particle-particle–mesh* ($P^3M$) [18] algorithms.

The second aim of this work is to focus on the key role which could be played by heterogeneous platforms to efficiently cope with complex computational problems. In this case, a heterogeneous platform, made by connecting a specialized architecture to a general-purpose platform, is used in a computationally intensive computational problem. The efficient use of the platform (induced by a suitable mapping of the algorithm onto the machine architecture and the use of a smart communication scheme) has allowed us to reach a sustained computational power of the order of 10 Gflops/s, necessary to perform extensive calculations.

The scheme of the paper is the following. The next section provides a brief outlook of the heterogeneous platform used to perform computations. The definition of the physical model considered for the computations is the object of the third section, which also contains a schematic layout of the techniques used to implement the calculations on the computing architecture. The fourth and the fifth sections are devoted to the presentation and the discussion of the results. In these sections both the scientific relevance of the resulting data and the fate of heterogeneous computing in complex scientific calculations are discussed.

## 2. LAYOUT OF THE COMPUTATIONAL PLATFORM

The heterogeneous platform used for computations is a MIMD–SIMD [19] platform, called PQE1 (Fig. 1), realized in the frame of an industrial program by ENEA and QSW (an Italian company of the Finmeccanica group) [20]. The PQE1 is a platform where the flexibility and the operability of a MIMD platform with a distributed-memory architecture are coupled to the power and the efficiency of SIMD machines. We assume that most algorithms arising in scientific applications are mainly expressible through synchronous programs with synchronous communications. These execute the same instruction on sets of different data, which can be easily mapped onto data parallel structures with regular

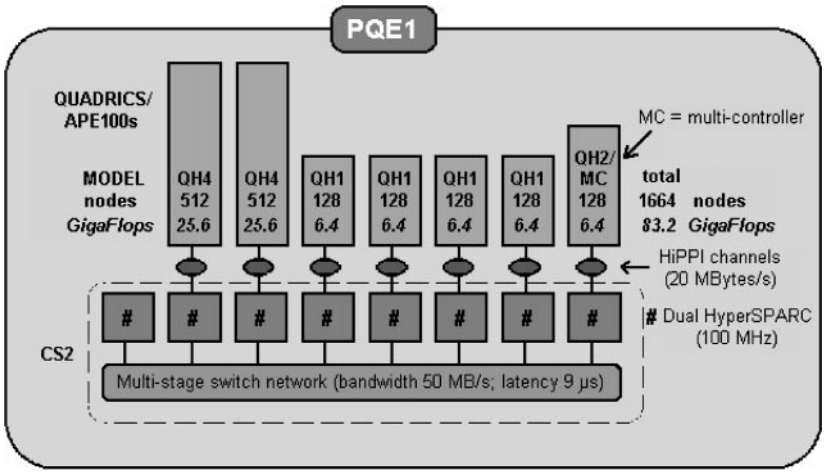


**FIG. 1.** Schematic layout of the PQE1 platform. The proprietary multistage switch network of the CS2 platform has a Fat Tree topology. Aside from the HiPPI channel, there is a transputer-based link which allows communications to occur between the CS2 node and the connected SIMD platform.

patterns of memory access. Under these assumptions, it is reasonable to allot those parts to the SIMD machine, leaving the remaining tasks of the computation to be executed on the MIMD part. The PQE1 platform consists of a MIMD general-purpose platform, acting as a docking unit, and of seven SIMD machines.

The MIMD system is a Meiko/QSW CS-2 platform with eight nodes, each of them based on a dual-HyperSparc processor at 125 MHz, connected in the SMP configuration by a Meiko/QSW proprietary network based on the Elan/Elite devices and implementing a multistage interconnection network with Fat Tree topology and a point-to-point bandwidth of 100 Mbytes/s. This platform offers a peak speed of 2.18 Gflops/s and has about 2 Gbytes of addressable RAM.

The SIMD platforms come from the APE project (APE100 [2, 3]) and have been produced by QSW with the commercial name of Quadrics. The installed platforms have the following characteristics: two of them (called QH4) have 512 floating point units (FPU) arranged as an $(8 \times 8 \times 8)$ 3D torus, and five of them (called QH1) have 128 FPUs arranged as an $(8 \times 4 \times 4)$ 3D torus. Each FPU is based on a custom VLIW processor, has a clock frequency of $\nu = 25$ MHz, and is able to terminate a "normal-operation" $AB + C$ (where $A$, $B$, and $C$ are IEEE 754 standard, single-precision, real numbers) every clock cycle. Each processor thus executes two floating point operations in one clock cycle (when the pipeline is full) and has a peak speed of 50 Mflops/s. Each FPU is connected to a data memory of 4 Mbytes and has an internal register file (RF) with 128 registers. Each clock cycle, the processor is able to read two operands from RF and write one result to RF. Communications with other adjacent FPUs, connected in the north, south, east, west, up, and down directions, are synchronous and memory mapped. The interprocessor communication bandwidth is 12.5 Mbytes/s, so the 512 (128) processor configuration has an aggregate bandwidth of 6.4 (1.6) Gbytes/s and a peak speed of 25.6 (6.4) Gflops/s.

The SIMD APE100/Quadrics machines are connected to the MIMD system through HiPPI (High-Performance Parallel Interface) channel, which provides a bandwidth of 20 Mbytes/s. Each MIMD node is connected to a different SIMD platform, as in the scheme of the complete prototype reported in Fig. 1. Looking at previous data, it is clear that

the machine is strongly unbalanced, having the highest computational and communication speed in the SIMD part.

The rationale for the design of such a prototype platform is related to the necessity of having a complex computing platform whose complexity mirrors that of the computational codes used in scientific applications. These latter are, in fact, formed by a sequence of tasks, each of them characterized by a *task granularity*, $g_t$, given by

$$g_t = \frac{N_{op}}{D_{I/O}}, \tag{1}$$

where $N_{op}$ is the number of floating point operations to be performed and $D_{I/O}$ is the amount of I/O data to be processed in the task. Analogously, it is possible to define a *machine granularity*, $g_m$, given by

$$g_m = \frac{F_{op}}{B}, \tag{2}$$

where $F_{op}$ is the computational power of the platform and $B$ its I/O bandwidth. It has been proved [23] that an efficient implementation of the task on a given computational platform implies that

$$g_m < \eta g_t, \tag{3}$$

where $\eta$ is a suitable factor $0 < \eta < 1$ expressing the efficiency of the task implementation. For this reason, an efficient implementation of a complex computational code implies the simultaneous presence of a complex computational structure able to satisfy the requirement of Eq. (3) for each task composing the code. The complexity of the PQE1 platform is thus exploited by allotting the high-granularity tasks to the SIMD part and the low-granularity and the pre/post-processing tasks to the MIMD machine. Incidentally, the estimate of the theoretical peak power speed of the complete (1664 processors) PQE1 machine is ~85 Gflops, which is significantly lower than the 1.08 Tflops of GRAPE4 [6]. Just the follow-up of the Quadrics/APE100 platform, which will be based on the APE1000 SIMD machine, will reach 1 Tflops (66-Mhz processors) and 1.6 Tflops (100 Mhz). By the way, as we show, even using part of the whole PQE1 system, it is possible to represent 128-K particle systems for tens of crossing times with acceptable accuracy.

## 3. MODEL AND COMPUTATIONS

We represent the stellar system as a set of $N = 128{,}000$ point-masses (stars) interacting via the classical pair gravitational potential

$$V(r_{ij}) = -G\frac{m_i m_j}{r_{ij}}, \tag{4}$$

where $r_{ij}$ is the distance between the $i$th and $j$th stars of the system. The stellar masses are assumed all equal. To avoid force divergence, a *smoothing* length $\epsilon$ is introduced, such that the replacement of $r_{ij}$ with $r'_{ij} = (r^n_{ij} + \epsilon^n)^{1/n}$ allows a mollification, dependent on the integer $n \geq 1$, of the interaction potential. The introduction of the smoothing parameter $\epsilon$

and the choice of $n$ affects the dynamics below and above that length scale. This parameter, in general, is set to values smaller than the average interparticle distance, in order to ensure an acceptable level of approximation of the system's dynamics. The choice of $n$ is, of course, arbitrary and depends on the type and level of smoothing one wants to reach. The choice $n = 2$ corresponds to the replacement of point-masses with Plummer's spheres of *core* radius $\epsilon$ (see Eq. (5)) and it is often used in the literature without any compelling reason ($\epsilon$ is always much larger than the stellar radius). We perform the computations presented in this paper using $n = 1$ and, for the sake of comparison, $n = 2$. The main differences in the family of smoothing potentials as dependent on $n$ are as follows: (i) once $\epsilon$ is fixed, in the limit $r \gg \epsilon$ the larger the $n$, the closer the smoothed potential to the Newtonian (of course, the same level of approximation can be reached with a smaller $n$ taking a smaller $\epsilon$); (ii) for $r_{ij} \to 0$ the (attractive) interaction force approaches zero whenever $n > 1$, while it tends to the limit $1/\epsilon^2$ when $n = 1$. Figure 2 shows the ratio between the intensities of the smoothed interaction force and the Newtonian as a function of the (true) distance between two particles in units of $\epsilon$. It should be noted how the force during close encounters is strongly underestimated: as reference, when $r_{ij} = \epsilon/100$, the force evaluated with $n = 1$, 2, 3, 4 is, respectively, a factor of $10^{-4}$, $10^{-6}$, $10^{-8}$, $10^{-10}$ smaller than the Newtonian. Point (ii) means that the particular choice $n = 1$ keeps some of the correct Newtonian sharpness of close encounters ($r_{ij}/\epsilon \leq 1$), as required when the smoothing, as in our case, is introduced just for computational convenience and *not* (as is often the case) to artificially

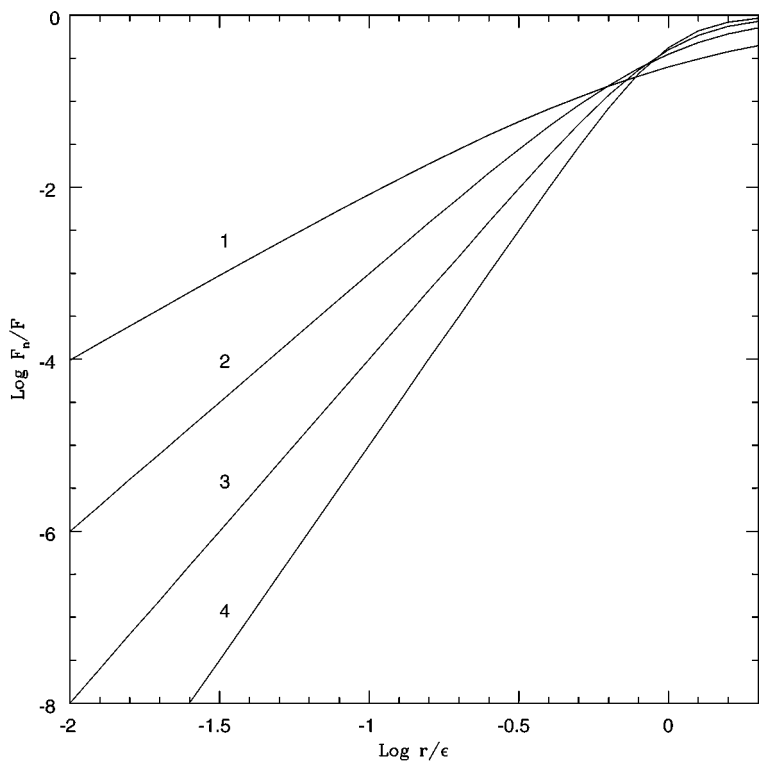


**FIG. 2.** The (logarithmic) ratio of the softened to the newtonian gravitational force between two particles, for four values of the exponent $n$ in the softening formula (which labels the curves) as a function of their distance (in units of the softening parameter $\epsilon$).

reduce the degree of *collisionality* of the system because the aim is to represent systems with large $N$ with a (much) smaller number of particles. Of course this choice implies a slower convergence to the Newtonian potential at larger scales (to have the same 90% approximation of the $n = 2$ case, an $\epsilon$ five times smaller is required).

In this paper (see Section 4) we present a set of computations performed using the simplest ($n = 1$) smoothing formula as reference, and, for the sake of comparison, the simulation of the evolution of the system with a massive black hole at its center has been done using, also, the $n = 2$ smoothed distance (keeping of course the same value of $\epsilon$).

When a massive object is present in the system (as a massive black hole) another length scale is naturally introduced into the problem: the tidal radius $r_t = (\frac{m_{BH}}{2m})^{1/3} R_*$. A star of mass $m$ and radius $R_*$ approaching a black hole (of mass $m_{BH}$) at a distance smaller than $r_t$ is destroyed by the strong tidal deformation, and consequently, its mass goes to increase that of the black hole, with a positive feedback on the tidal radius. Our computational code takes into account the possibility that a star is swallowed by the massive object which, accordingly, increases its mass and its $r_t$. However, $r_t$ is usually much smaller than the typical interstellar distance, so that $m_{BH}$ remains almost unchanged throughout the simulations.

The initial spatial distribution of the $N$ stars of equal masses has been sampled by a spherical Plummer distribution (see [22]),

$$\rho(r) = \frac{\rho_0}{\left[1 + \left(\frac{r}{r_c}\right)^2\right]^{\frac{5}{2}}}, \tag{5}$$

where the central density $\rho_0$ and the "core" radius $r_c$ are free parameters. The initial stars velocities have been obtained self-consistently from the velocity distribution function that generates the Plummer's density law,

$$f(\mathbf{r}, \mathbf{v}) = \begin{cases} (-E)^{7/2}, & E \leq 0 \\ 0, & E > 0, \end{cases} \tag{6}$$

where $E = 1/2v^2 - \phi(r)$ is the individual star's energy in the (spherical) potential $\phi(r)$ given by the Plummer mass distribution. The star velocities distributed according to Eq. (6) are scaled to have a virial ratio $Q = 2T/|\Omega| = 0.964$ (where $T$ and $\Omega$ are the kinetic and the gravitational energies of the system) where the equilibrium value is 1; the inclusion of a black hole with a mass 0.02 and 0.1 of the total star mass at the center of mass changes the virial ratio to $Q = 0.87$ and $Q = 0.75$, respectively, inducing a stronger gravitational collapse.

The equations of motion have been integrated by using the central difference Verlet-scheme [21] with a fixed time step. This scheme allows an accuracy of the order of $\Delta t^4$ in the positions and $\Delta t^2$ for the velocities. The time-step $\Delta t$ has been empirically selected by requiring the relative error of the total energy to be smaller than $10^{-4}$ per time step. After the value of $\epsilon$ was fixed several simulations were carried out, using different values of $\Delta t$, up to the value which allowed the relative error of the total energy in the desired range to be obtained.

The part of the PQE1 platform selected for the calculations consists of a single MIMD node and a QH4 platform. The MIMD node has been used to perform data initialization, the evaluation of the component of the star forces arising from the interaction with the black

hole, the solution of the equations of motion, and the evaluation of the relevant physical quantities (total and potential energy, virial ratio, Lagrangian radii, and mass and velocity distributions). The $O(N^2)$ force-loop has been, in turn, implemented on the QH4 platform. For this purpose, a number of stars, $N_p = N/n_p$ (where $n_p = 512$ is the number of FPUs of the QH4 platform), have been allotted to each FPU. The force calculation has been performed by making use of a recently developed hypersystolic algorithm [24] in order to exchange data among the processors. This scheme allows reduction of the redundancy typical of the systolic algorithm [25], thus allowing savings of a substantial amount of computing time.

In systolic-type algorithms, there is a regular sequence of calculation and communication steps. In our case, after the allocation of equal groups of $N_p$ stars on each FPU, the code evaluates the $N$-body forces within each group. A copy of the positions of each group is then moved, from the initial to the next-neighbor FPU, and, there, is interacted with the resident group of stars. The process is repeated until each group of stars has visited each others FPU. On each FPU is thus accumulated the force acting on the resident group of stars.

The $O(N^2)$ problem requires, given $N$ data elements (coordinates and masses of the $N$ stars) being distributed among $p$ processors, $O(Np)$ of interprocessor communications (i.e., $O(N)$ communications per processor). As this often leads to severe performance bottlenecks, it is mandatory to search for new algorithms that are able to reduce interprocessor communications to a number $O(N)$ per processor.

The hypersystolic algorithm, recently introduced, has the potential to decrease interprocessor communications for computational problems of the type mentioned above to a number $O(N^{\frac{1}{2}})$ per processor. This is achieved by a 1-dimensional systolic mapping of the data onto the processing elements and by the use of shortcut interprocessor communication (hyperconnections) together with a replicated systolic mapping of data.

The basic feature of hypersystolic computing is a sequence of shifts called HS-base, which represent the hypersystolic strides along the 1-dimensional chain to be performed in the hypersystolic parallel calculation. The direct computation of *optimal* bases is exponentially expensive, with the number of processors $p < 64$. For larger numbers of processors, hitherto, aside from the so-called *regular* bases, new HS-bases have been determined [26] with a search technique based on simulated annealing.

The implementation of the hypersystolic communication scheme on the $N^2$ calculation on the 512-node Quadrics QH4 has allowed about a 20% improvement in interprocessor communication compared to the regular base implementation.

The chosen implementation strategy allows exploitation of a double level of parallelism: the first consisting of the parallel implementation of the interstellar force calculation in the SIMD platform by the hypersystolic algorithm; the second related to the concurrent black hole–stars force calculation performed by the host platform during the time spent by the SIMD machine to produce the interstellar force.

The machine performance was such that it allowed an execution time $t_{ex} = 120$ s for the calculation of the single time step of the cluster dynamics, by using the mentioned PQE1 partition. About 20% of this time is related to different communication actions (to/from the SIMD machine and within the SIMD machine, in the hypersystolic loop), the residual time being spent on number crunching. The efficiency of the SIMD code (in terms of efficiency of use of single FPU resources) was around 30%, thus leading to a sustained computational power, in the SIMD part, of about 9 GFlops/s.

## 4. COMPUTATIONAL DETAILS AND RESULTS

Three model systems have been simulated, all of them containing $N = 128{,}000$ masses. The first one represents the globular cluster without any massive object; this system has been retained as reference and its behavior compared to that of the other systems. The second system contains a black hole of mass $m_{BH} = 0.02$ (in units of the total star mass) located at the center of mass of the cluster. The third system contains a black hole with $m_{BH} = 0.1$.

As we explained in Section 3, all three simulations were performed with a smoothed distance of the form $r'_{ij} = r_{ij} + \epsilon$ in the interaction potential; the third simulation ($m_{BH} = 0.1$) was performed also with the Plummer's potential (i.e., $r'_{ij} = (r_{ij}^2 + \epsilon^2)^{1/2}$). This was done to compare the effect of a difference in the smoothing formula on the overall dynamical evolution of such a system, which we expect not to be relevant for average quantities, such as the one discussed in the following, as confirmed also by a comparison of figures (see Figs. 10, 14, 15, 16).

We express the model parameters taking as units of length and mass the initial radius of the system and its total mass, respectively. Moreover, setting $G = 1$ implies that $t_c$ is the time unit. In these units, the value of $\epsilon = R/500 = 0.002$ that we choose is much smaller (one-tenth) than the average interparticle distance (which is $\propto n_*^{-1/3}$, with $n_*$ being the average number density); this guarantees an acceptable spatial resolution and keeps the newtonian behavior of the interparticle force. In the case of the unperturbed cluster (without the black hole), a $\Delta t = t_c/250$ has been used. The constraint imposed on the numerical scheme to ensure an energy conservation of at least $10^{-4}$ per time step implied the use of a smaller time step ($\Delta t = t_c/500$) when a massive black hole was present. This is clearly due to the violent dynamics induced by a black hole whose mass is 2,560 and 12,800 times the individual stellar mass. The systems have been simulated over a time interval of 10 or 20 crossing times.

Figure 3 shows the time behavior of a relative error in the mechanical energy of a system without a central black hole. The error grows quickly (up to 1.8%) in the first crossing time,

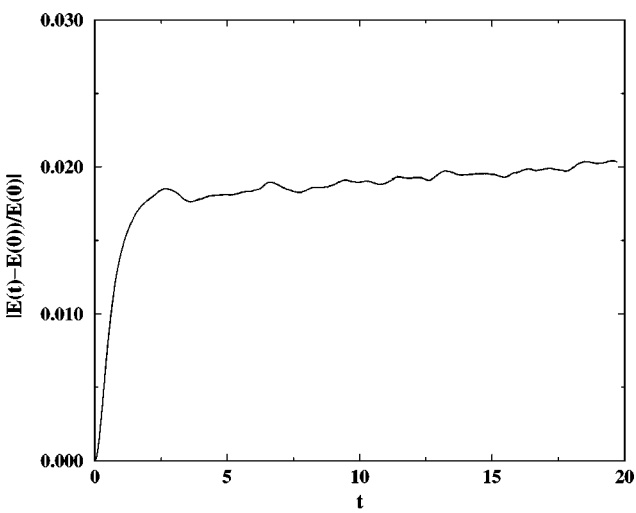


**FIG. 3.** The absolute value of the relative error in energy as a function of time (in units of crossing times) for a system without a black hole.

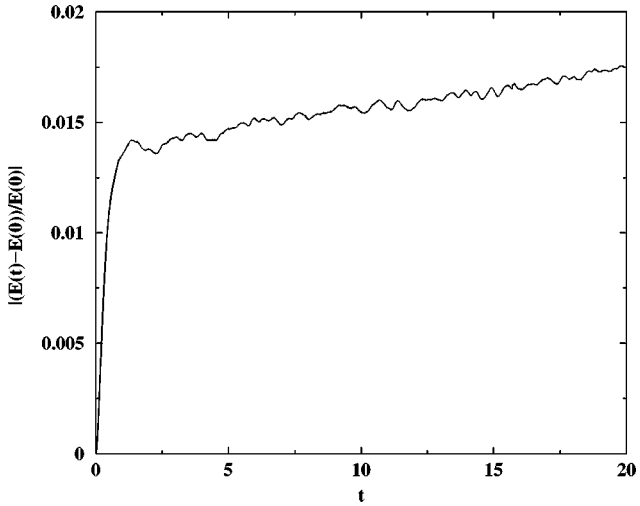


**FIG. 4.** The absolute value of the relative error in energy as a function of time (in units of crossing times) for a system with a black hole of mass $m_{BH} = 0.02$.

the error being induced by the overall dynamics; later, it increases very slowly, so that its extrapolation up to a two-body relaxation time (i.e., $\sim 1,000\ t_c$) yields a still-reasonable energy error of the order of 20%. As shown by Figs. 4 and 5, the presence of a black hole in the system causes increasing problems in energy conservation: with the chosen time step, in the case of $m_{BH} = 0.02$, the error, after 20 $t_c$, is of the order of 1.75%, while in the case of $m_{BH} = 0.1$ it grows up to 6.5%.

A relevant global indicator of dynamical activity of an $N$-body system is the virial ratio $Q = 2T/|\Omega|$ of the system. This quantity provides a first picture of the global dynamics in the cluster driven by the initial unbalance between kinetic and potential energy. The virial

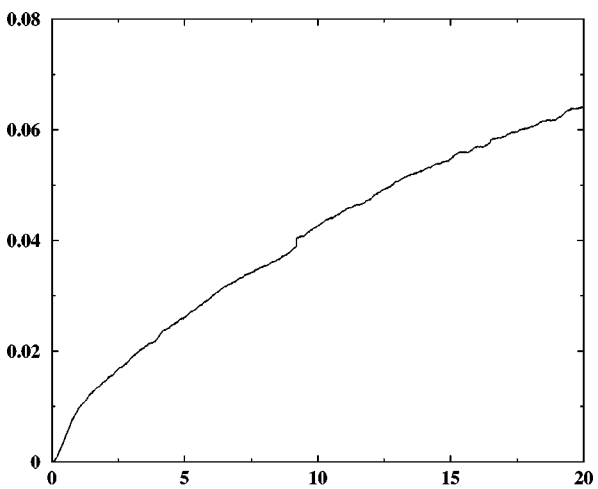


**FIG. 5.** The absolute value of the relative error in energy as a function of time (in units of crossing times) for a system with a black hole of mass $m_{BH} = 0.1$.

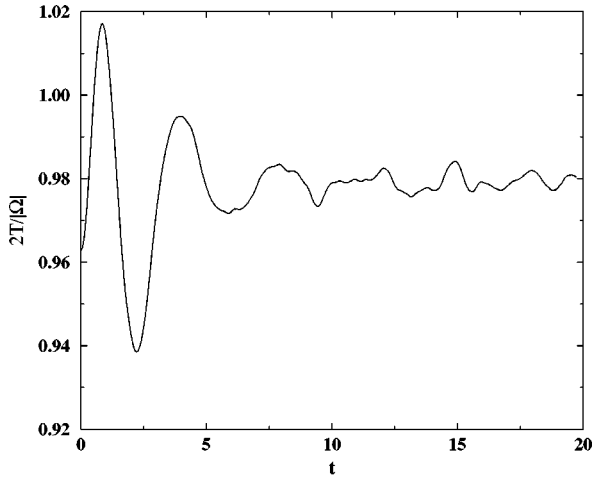


**FIG. 6.** Virial ratio, $2T/|\Omega|$, as a function of time for a system without a black hole. Time is expressed in units of crossing time, $t_c$.

ratio is strongly perturbed by the presence of the massive object. This produces a strong driving force, which brings the mass distribution to a virial equilibrium that is slightly different from $Q = 1$ due to the nonhomogeneity of the interaction potential function induced by the presence of the softening parameter $\epsilon$ (the larger the $\epsilon$, the lower the $Q$ value at virial equilibrium). As an example, we report in Fig. 6 the time evolution of $Q$ for the case of a system without a black hole. For the most massive black hole here considered ($m_{BH} = 0.1$), the virialization occurs more violently.

The virialization process is due to a violent relaxation that occurs as a consequence of a series of damped (nonadiabatic) oscillations of the system (see Fig. 7). Virialization is reached after three to five crossing times.

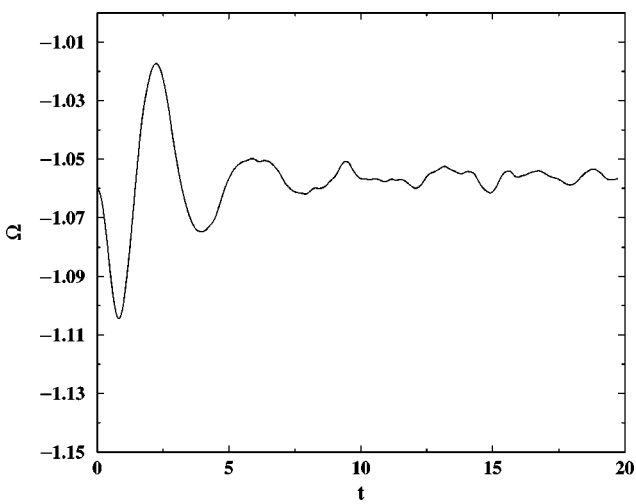


**FIG. 7.** Total potential energy Ω vs time for a system without a black hole. Time is expressed in units of crossing time, $t_c$.

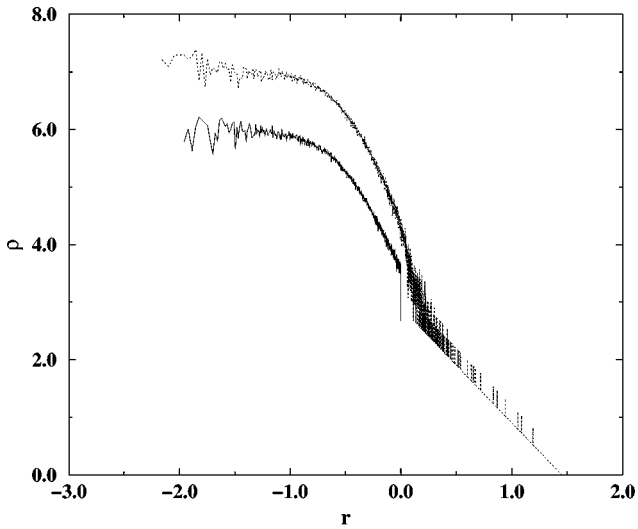


**FIG. 8.** Mass density of a system as a function of the distance from the center (in logarithmic scales and in model units), in the case of a system without the black hole, at $t = 0$ (lower curve) and at $t = 10\,t_c$ (upper curve). The curve at $t = 10\,t_c$ has been shifted upward 1 dex for the sake of a better comparison.

The evolution of both the spatial and projected density radial distributions is shown in Figs. 8 to 11, where the initial and virialized ($t = 10\,t_c$) profiles are reported. The time evolution leads to a steepening of the profile toward the cluster center ($r < 0.1$), which is more pronounced at a larger black hole mass, and to the population of a "halo" ($r > 1$) of high-velocity stars. Both the external profile and the inner one (the latter evolving, of course, just in the presence of the central compact object) are attained in a short time, on the order of one crossing time.

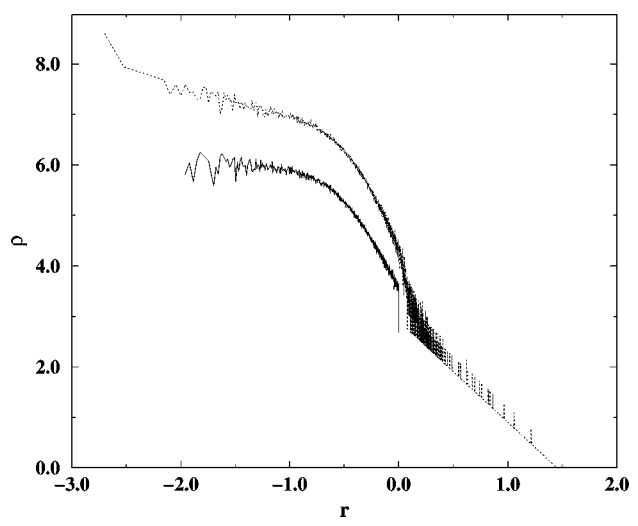


**FIG. 9.** Mass density of the system as a function of the distance from the center (in logarithmic scales and in model units) in the case $m_{BH} = 0.02$ at $t = 0$ (lower curve) and at $t = 10\,t_c$ (upper curve). The curve at $t = 10\,t_c$ has been shifted upward 1 dex for the sake of a better comparison.

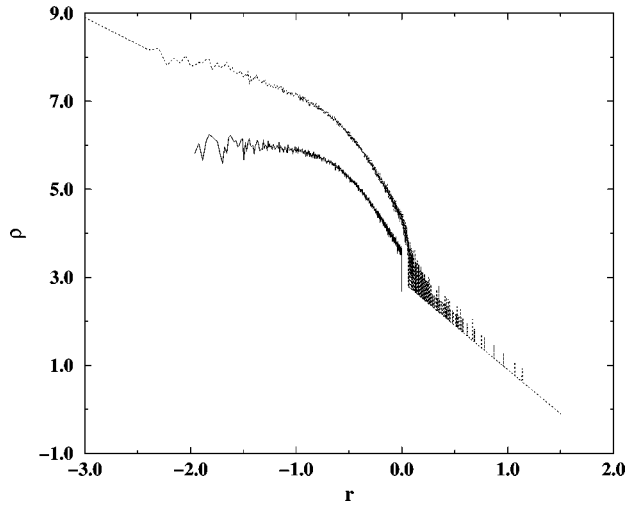


**FIG. 10.** Mass density of the system as a function of the distance from the center (in logarithmic scales and in model units) in the case $m_{BH} = 0.1$ at $t = 0$ (lower curve) and at $t = 10\,t_c$ (upper curvere). The curve at $t = 10\,t_c$ has been shifted upward 1 dex for the sake of a better comparison.

The slope of the space density inner distribution is for $m_{BH} = 0.1$ at $t = 10\,t_c$, $-0.92$ as shown in Fig. 10 (i.e., intermediate between the values $-3/2$ and $-1/2$, characteristic, respectively, of the density cusps analytically (and approximately) evaluated for the distribution of stars bound to a black hole and of those unbound [16]). We note that the slope of the halo region closely matches the expected $r^{-2}$ profile (see, for instance, [27]).

The dynamical evolution of the model clusters is also characterized by the appearance of some anisotropy in the velocity distribution in the external regions. This has been

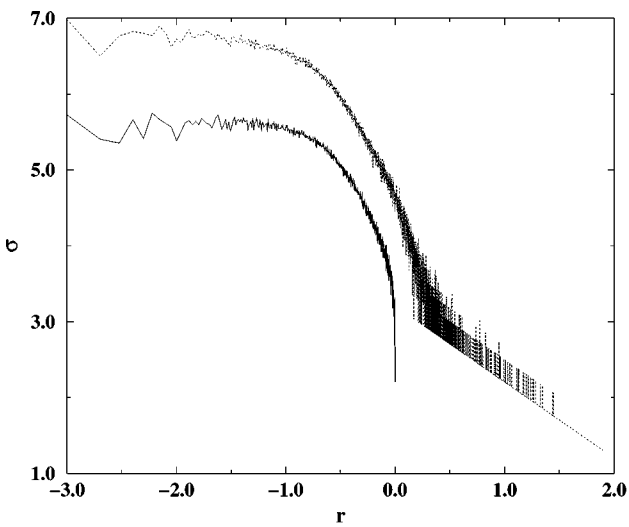


**FIG. 11.** Projected mass density of the system as a function of the distance from the center (in logarithmic scales and in model $m_{BH} = 0.1$, at $t = 0$ (upper curve) and at $t = 10\,t_c$ (lower curve). The curve at $t = 10\,t_c$ has been shifted upward of 1 dex for the sake of a better comparison.

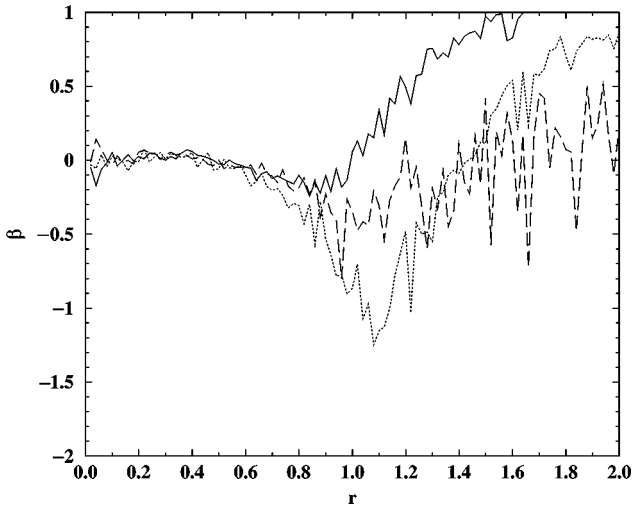


**FIG. 12.** Anisotropy parameter $\beta$ (in model units) for the $\theta$ component of the velocity for the system without the black hole at $t = 0.2\,t_c$ (solid line), $t = 1\,t_c$ (dotted line), $t = 10\,t_c$ (dashed line).

characterized by the evaluation of the anisotropy parameters

$$\beta_\theta = 1 - \frac{\langle v_\theta^2 \rangle}{\langle v_r^2 \rangle},$$

$$\beta_\phi = 1 - \frac{\langle v_\phi^2 \rangle}{\langle v_r^2 \rangle},$$

(the averages in angle brackets represent the dispersions of the polar components of the velocity) as functions of the radial distance (see Figs. 12, 13, 14, and 16). Because the initial distribution function given by Eq. (6) is only dependent on the energy, the initial

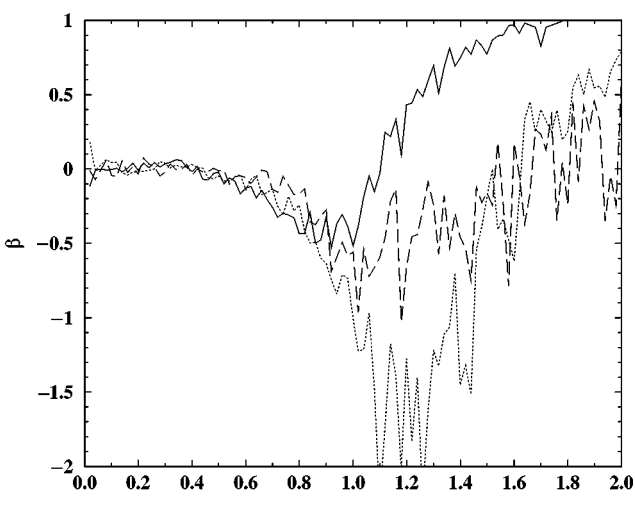


**FIG. 13.** Anisotropy parameter $\beta$ (in model units) for the $\theta$ component of the velocity for the system with $m_{BH} = 0.02$ at $t = 0.2\,t_c$ (solid line), $t = 1\,t_c$ (dotted line), $t = 10\,t_c$ (dashed line).

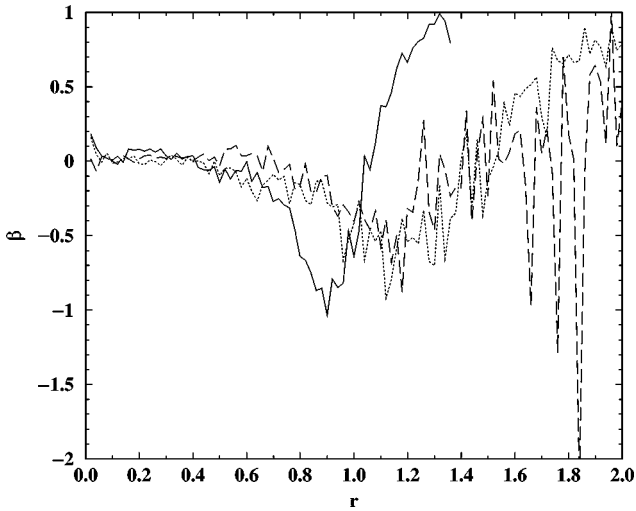


**FIG. 14.** Anisotropy parameter $\beta$ (in model units) for the $\theta$ component of the velocity for the system with $m_{BH} = 0.1$ at $t = 0.2\,t_c$ (solid line), $t = 1\,t_c$ (dotted line), $t = 10\,t_c$ (dashed line).

velocity distribution is obviously isotropic, and both $\beta_\theta$ and $\beta_\phi$ are zero (the three polar components of the velocity being the same, on the average). The behavior of $\beta_\theta$ and $\beta_\phi$ is very similar, and we expect that evolution keeps the velocity vector invariant for rotations on the plane orthogonal to the radial direction. We have thus plotted just $\beta_\theta$. In all the cases studied, a rapid increase in $\beta_\theta$ is evident in the outer regions, where, indeed, orbits are more radially pointed due to the expansion of the stellar halo. Moreover, we note that the more massive the central object, the more evident the negative minimum of the anisotropy parameter around the initial boundary at short times. In the case of $m_{BH} = 0.1$, the transverse

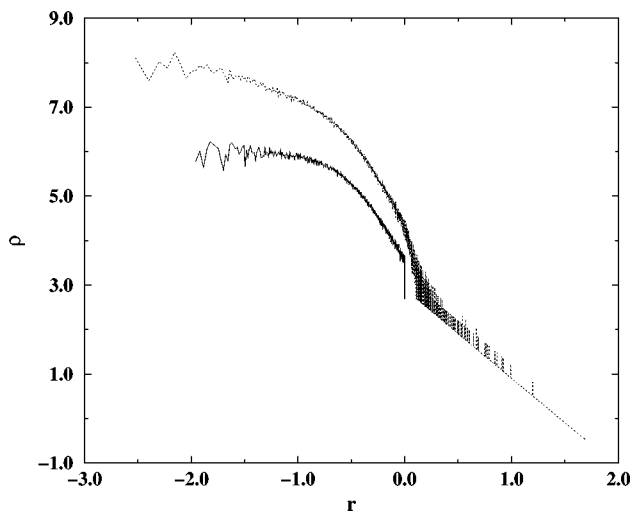


**FIG. 15.** Mass density of the system as a function of the distance from the center (in logarithmic scales and in model units) in the case $m_{BH} = 0.1$ at $t = 0$ (lower curve) and at $t = 10\,t_c$ (upper curve). The curve at $t = 10\,t_c$ has been shifted upward of 1 dex for the sake of a better comparison. In the smoothing potential $n$ is set equal 2.

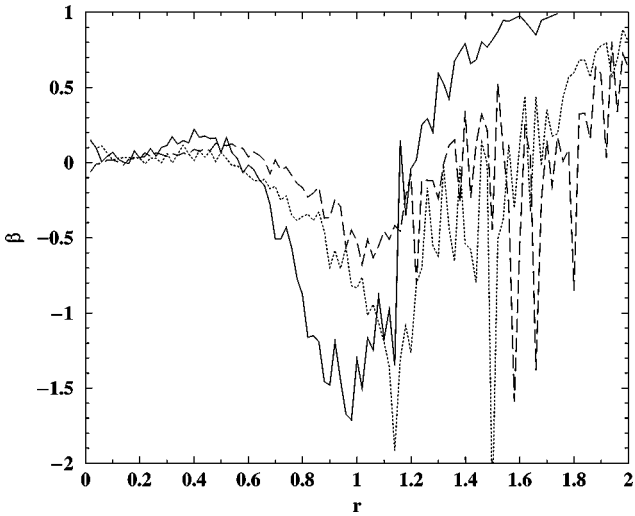


**FIG. 16.** Anisotropy parameter $\beta$ (in model units) for the $\theta$ component of the velocity for the system with $m_{BH} = 0.1$ at $t = 0.2\,t_c$ (solid line), $t = 1\,t_c$ (dotted line), $t = 10\,t_c$ (dashed line). In the smoothing potential $n$ is set equal 2.

components of the velocity dominate the radial ones, so $\beta \simeq -1$; this means that a quick effect of the instability caused by the massive object is that the transverse "temperature" doubles the radial. This seems a transient effect because, as the evolution goes on, the radial dependence of the $\beta$ parameter tends to be rather insensitive to the mass of the central object. At $t = 10\,t_c$, the isotropy is partially restored on the average, a radially biased distribution of orbits on the outskirts being still evident.

Finally, Fig. 17 is a snapshot, at $t = 10\,t_c$, of the star distribution projected onto a coordinate plane of the model cluster having the $m_{BH} = 0.1$ black hole at its center.

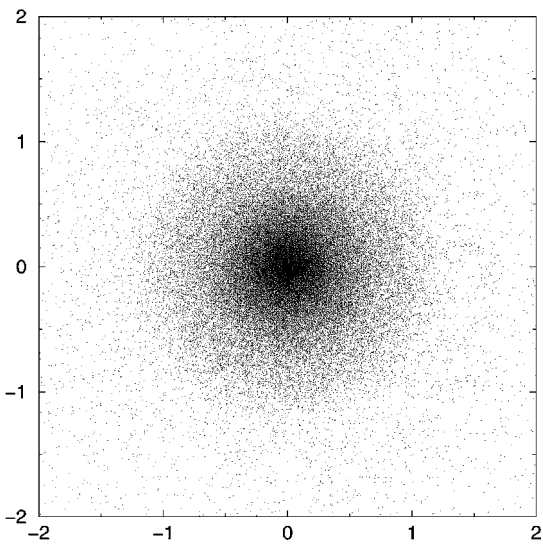


**FIG. 17.** Two-dimensional plot (restrained to the region containing the bulk of the mass distribution) showing the structure of a globular cluster with $m_{BH} = 0.1$, at $t = 10\,t_c$.

## 5. DISCUSSION AND CONCLUSIONS

Concerning the main questions which have stimulated this work, it is possible to draw two conclusions. First, the *heterogeneity* of the PQE1 platform can provide significant benefits in the gravitational $N$-body calculations, although the structure of the computational problem is very different from that for which the SIMD platform Quadrics/APE100 was conceived. This result confirms the relevance of the relation of Eq. (3), which should be considered the most important constraint to be fulfilled in the mapping of a code onto a computational platform.

The reported data confirm, in fact, that the increase in computational efficiency provided by heterogeneous platforms (where different architectures can coexist and provide an ideal computational frame to execute different parts of the complex computing codes characterized by different algorithmic complexity) can be seen as a key feature for high-performance computing, whose benefits should be more attentively searched and exploited.

The achieved sustained computational power allows the simulation of the dynamics of one crossing time (with $N = 128{,}000$) using a wall clock time of the order of $6 \times 10^4$ s; this figure allows simulations of the order of tens of crossing times. The new SIMD machine, derived from the INFN project APEmille and constituting the follow-up of the Quadrics/APE100 platform, will enhance the computational power by a factor of 10. This will permit a study of the evolution of the cluster over a time of the order of hundreds of crossing times (i.e., of the order of the two-body relaxation time).

The second conclusion is that from the astrophysical point of view, this work has introductory relevance to the "direct" study of the dynamics of populous stellar systems (up to the scale of globular clusters) whose internal densities vary over a range of scales such that approximations in the interaction potential (as multipolar expansions, solutions to Poisson's equation on a grid, etc.) are of questionable reliability. By the way, this work has shown how the inclusion of a massive object in a quasiequilibrium model of a globular cluster, represented as a set of $N = 128{,}000$ stars interacting with the "exact" potential (even if smoothed on a scale on the order of $1/10$ the average interstellar distance), has consequences to the overall dynamics. It induces a violent relaxation within a few crossing times, corresponding to an evolution of the star radial distribution toward a central peaked distribution close to $\rho \propto r^{-1}$ in the case of the most massive black hole considered ($m_{BH} = 0.1$ times the total stellar mass). Another effect enhanced by the presence of the massive object is the loss of isotropy in the velocity distribution, both in the outer regions, where radial orbits dominate, and in an intermediate zone, where, on the other hand, transverse components of the velocity prevail. The inner region stands isotropic throughout the evolution.

## ACKNOWLEDGMENTS

The authors kindly acknowledge discussions and suggestions from R. Spurzem and M.Hemsemdorf (ARI, Heidelberg), P. Miocchi and P. Di Matteo (Univ. of Roma), and P. Spinnato (DAS, Amsterdam). P. Palazzari and M. Coletta (ENEA, Roma) are gratefully acknowledged for their help in the implementation of the hypersystolic algorithm. Part of this work has been supported by a INFN/PQE2000 grant to one of us (NP), performed in the frame of the PQE1 project (ENEA–QSW) and partially supported by CASPUR.

## REFERENCES

1. *Accelerated Strategic Computing Initiative*, available at http://www.llnl.gov/asci.
2. A. Bartoloni, G. Bastianello, C. Battista, S. Cabasino, F. Marzano, P. S. Paolucci, J. Pech, F. Rapuano, E. Panizzi, R. Sarno, G. M. Todesco, M. Torelli, W. Tross, P. Vicini, N. Cabibbo, A. Fucci, and

R. Tripiccione, The hardware implementation of the APE100 architecture, *Int. J. Mod. Phys. C* **4**, 969 (1993).

3. A. Bartoloni, G. Bastianello, C. Battista, S. Cabasino, F. Marzano, P. S. Paolucci, J. Pech, F. Rapuano, E. Panizzi, R. Sarno, G. M. Todesco, M. Torelli, W. Tross, P. Vicini, N. Cabibbo, and R. Tripiccione, The software of the APE100 processor, *Int. J. Mod. Phys. C* **4**, 955 (1993).
4. I. V. Arsenin, Architectural choices for the Columbia 0.8 Teraflops machine, *Nucl. Phys. B* (*Proc. Suppl.*) **42**, 902 (1995).
5. J. Makino, M. Taiji, T. Ebisuzaki, and D. Sugimoto, GRAPE-4: A massively parallel special-purpose computer for collisional $N$-body simulations, *Astrophys. J.* **480**, 432 (1997).
6. J. Makino and M. Taiji, *Scientific Simulations with Special-Purpose Computers: The GRAPE Systems* (Wiley, New York, 1998).
7. R. Spurzem, Direct $N$-body simulations, *J. Comput. Appl. Math*. **109**, 407 (1999).
8. H. R. Swendsen and J. S. Wang, Nonuniversal critical dynamics in Monte Carlo simulations, *Phys. Rev. Lett*. **58**, 86 (1987).
9. A. L. Talapov, L. N. Shchur, H. W. J. Blöte, and N. Shchur, Cluster algorithm special purpose computer for the three-dimensional Ising model, *JETP Lett*. **62**, 174 (1995).
10. S. Shirakawa, T. Yoshii, K. Murakami, U. Nagashima, S. Obara, T. Amisaki, K. Kitamura, H. Takashima, and K. Tanabe, *The Architecture of Molecular Orbital Calculation Engine (MOE)* (IEICE, 1996), Technical Report CPSY96-46, pp. 45–50.
11. *The C4 Cluster*, available at http://igc.ethz.ch/c4/C4-cluster.html.
12. N. Pucello, M. Rosati, G. D'agostino, F. Pisacane, V. Rosato, and M. Celino, Search of molecular ground state via genetic algorithm: Implementation on a hybrid SIMD–MIMD platform, *Int. J. Mod. Phys. C* **8**, 239 (1997).
13. P. Palazzari, L. Arcipiani, M. Celino, R. Guadagni, A. Marongiu, A. Mathis, and P. Novelli, Heterogeneity as key feature of high performance computing: The PQE1 prototype, in *IEEE Proceedings of the 9th Heterogeneous Computing Workshop, May 1, 2000, Cancun, Mexico* (IEEE Press, 2000).
14. R. Lorenzini, L. Delle Monache, G. Zanini, M. C. Cirillo, M. Celino, and P. Palazzari, Porting of the chemical module of callgrid code on a SIMD massive platform, in *Advances in High Performance Computing: Proceedings of the High Performance Computing 1997 (HPC97), Santiago de Compostela, 2-4 July 1997*, edited by H. power and J. J. Casares Long (Computational Mechanics Publications, 1997).
15. V. Rosato and M. Rosati, unpublished results.
16. J. Binney and S. Tremaine, *Galactic Dynamics* (Princeton Univ. Press, Princeton, NJ, 1987), Princeton Series in Astrophysics.
17. J. Barnes and P. Hut, A hierachical $O(N \log N)$ force-calculation algorithm, *Nature* **324**, 446 (1986).
18. R. W. Hockney and J. W. Eastwood, *Computer Simulation Using Particles* (Hilger, Bristol, 1988).
19. The acronyms MIMD and SIMD refer to parallel platforms working asynchronously (multiple instructions, multiple data) and synchronously (single instruction, multiple data).
20. *HPC Resources: PQE-1*, available at www.pqe2000.enea.it/home/pqe1/PQE1_a.html.
21. L. Verlet, Computer "experiments" on classical fluids. I. Thermodynamical properties of Lennard–Jones molecules, *Phys. Rev.* **159**, 98 (1967).
22. B. C. Plummer, On the problem of distribution in globular star clusters, *Mon. Not. Roy. Astron. Soc*. **71**, 460 (1911).
23. P. Palazzari and P. D. Atanasio, Electromagnetic simulations through the PQE1 hybrid parallel architecture, in *Advances in Computation: Theory and Practice* (Nova Science Ed., 2001), to appear.
24. T. Lippert, U. Glasser, H. Hoeber, G. Ritzenhofer, K. Shilling, and A. Seyfried, Hyper-systolic processing on APE100/Quadrics: $n^2$-loop computations, *Int. J. Comput. Phys. C* **7**, 485 (1996).
25. N. Petkov, *Systolic Parallel Processing* (North-Holland,Amsterdam 1992).
26. P. Palazzari, T. Lippert, and K. Shilling, Hyper-systolic processing on the Quadrics: Improving inter-processor communication by simulated annealing, in *Advances in High Performance Computing*, edited by L. Grandinetti, J. Kovalik, and M. Vajtersic (Kluwer Academic Publishers, Dordrecht/Norwell, MA, 1997), Nato ASI Series.
27. S. L. Shapir and A. P. Lightman, The distribution of stars around a massive black hole, *Nature* **262**, 743 (1976).